Available online at www.sciencedirect.com

SCIENCE DIRECT®

Engineering Geology 81 (2005) 213–226

ENGINEERING GEOLOGY

www.elsevier.com/locate/enggeo

Expansive bentonite–sand mixtures in cyclic controlled-suction drying and wetting

E.E. Alonso, E. Romero *, C. Hoffmann, E. García-Escudero

Department of Geotechnical Engineering and Geosciences, Universitat Politècnica de Catalunya, UPC, c/ Jordi Girona 1-3, Building D-2, 08034 Barcelona, Spain

Available online 11 August 2005

Abstract

Expansive clay buffers in radioactive waste disposal designs experience cyclic drying and wetting paths during different stages of their design life. Clayey soils subjected to these processes develop swelling and shrinkage deformations, which give rise to the accumulation of compression or expansion strains during suction cycles. Experimental studies were undertaken using oedometer tests on an artificially prepared bentonite–sand mixture (80% bentonite by dry mass). In order to study these processes and to identify the most important features controlling soil behaviour, several wetting–drying cycles with suctions ranging between 130 and 4 MPa were applied using vapour equilibrium technique and covering a wide range of over-consolidation ratios (OCR). The tested samples showed cumulative shrinkage strains along the successive cycles, which became more significant at increasing vertical net stresses (low OCR values). However, no accumulation of expansion strains was detected at elevated OCR values. Test results were interpreted and predicted within the context of an elastoplastic model proposed by Alonso et al., 1999, [Alonso, E.E., Vaunat, J., Gens, A., (1999). Modelling the mechanical behaviour of expansive clays. Engineering Geology, 54, 173–183.] which takes into account the accumulation of strains. A good correspondence between measured soil response and model predictions was observed. The paper also presents the methodology to derive the constitutive parameters.

Keywords: Swelling; Shrinkage; Suction; Expansive clay; Model

1. Introduction

Soils are naturally subjected to cyclic and strong drying and wetting paths due to natural environmental fluctuations. Buffers constructed using clays of expansive nature in radioactive waste disposal designs also experience stress and suction cycles during different stages of their design life. In a general case, stress and suction paths are far from being a simple monotonic

* Corresponding author. Geotechnical Laboratory, Departamento de Ingeniería del Terreno, Jordi Girona 1-3, Edificio D-2, Universitat Politècnica de Catalunya, 08034 Barcelona, Spain. Tel.: +34 93 4016888; fax: +34 93 4017251.

E-mail address: enrique.romero-morales@upc.edu (E. Romero).

0013-7952/$ - see front matter © 2005 Elsevier B.V. All rights reserved.
doi:10.1016/j.enggeo.2005.06.009

process. Clayey soils undergo an increase in volume during water uptake, but also experience an important amount of shrinkage on water removal, which give rise to the accumulation of compression or expansion strains during suction cycles. Several studies were undertaken in the past; however, few experimental studies have been reported in the literature with respect to water transfer in vapour form under controlled-suction conditions. In fact, vapour transfer plays a major role in buffers of radioactive waste disposal designs because of the existing strong thermal gradients. In addition, bentonite-based buffers develop very large suctions, which cannot be tested using conventional techniques with liquid water transfer, such as the axis translation and osmotic techniques. Furthermore, the response of expansive soils against suction cycles is a key information required to understand its constitutive behaviour.

Experimental results describing the volume change response of expansive soil exposed to cyclic wetting and drying have been reported by Dif and Bluemel (1991) and Al-Homoud et al. (1995), who detected 'fatigue' of swelling (shrinkage accumulation) that increases at higher vertical stresses. This behaviour was explained in terms of a continuous rearrangement of soil particles, leading to a less active microstructure. On the other hand, Obermeier (1973), Popescu (1980) and Pousada (1984) observed an opposite effect, in which the amount of swelling increased with the number of cycles. Day (1994) and Basma et al. (1996) reported cumulative shrinkage or expansive strains, depending on the suction reached during the drying paths.

The objectives of the research presented in this paper are focused on the investigation and prediction of the volume change response of an artificially prepared mixture of bentonite and sand subjected to several wetting and drying cycles in the high suction range. To achieve the first objective, an experimental programme was designed in which several controlled-suction wetting and drying cycles, with suctions ranging between 130 and 4 MPa, were applied using vapour equilibrium technique. Oedometer tests were performed under different values of constant vertical net stress covering a wide overconsolidation (OCR) range. To address the second objective, the volume change response of the mixture is discussed and interpreted within the context of the elastoplastic model proposed by Alonso et al. (1999) (BExM: Barcelona Expansive Model). Comparisons are provided between the experimental results and the predicted results. Based on these studies model parameters are derived.

2. Experimental programme

2.1. Tested material

Tests were performed on statically compacted bentonite–sand mixtures. This material was selected due to the following favourable properties: significant volume changes on suction cycles and an appropriate water permeability, which allowed the time required for equalisation to be kept within reasonable bounds. Bentonite powder was mixed with silica sand to achieve a dry mass ratio of 80% bentonite and 20% sand. Ca-bentonite powder passing ASTM No.40 (FEBEX bentonite, ENRESA, 2000) presents a liquid limit of 93%, a plastic limit of 47%, 45% of particles less than 2 μm and a density of solid particles of 2.70 Mg/m^3. The uniform sand passing ASTM No.16 presents a uniformity coefficient of $C_u = 2$ and an effective size of $D_{10} = 0.21$ mm.

The mixture in powder form was allowed to equilibrate at an average relative humidity of 55% (suction of $s = 80$ MPa) to achieve a hygroscopic water content of 10.5%. Specimens (30 mm in diameter and 8 mm high) were then statically and one-dimensionally compacted at a displacement rate of 0.2 mm/min and constant water content to a target dry density of around 1.5 Mg/m^3. The initial degree of saturation was around 35%.

A complementary test programme under oedometer conditions was also performed to obtain additional constitutive information on the mechanical behaviour of the as-compacted state. These tests include wetting at constant volume (swelling pressure tests) and loading–unloading paths at constant suction. Based on these results compressibility parameters and yield properties of the material were estimated. Fig. 1 shows the oedometer loading–unloading test performed at constant suction $s = 80$ MPa (as-compacted state). A clear pre- and post-yield response is detected, defining a preconsolidation stress at around 5 MPa. Fig. 2 represents the swelling

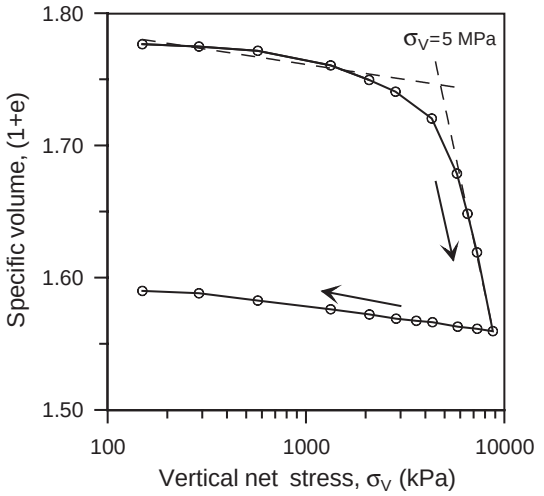

Fig. 1. Loading–unloading test at constant suction $s=80$ MPa on the as-compacted sample.

pressure test performed under constant volume conditions. Imbibition of the sample was performed by liquid transfer at constant head. Water inflow was registered by a burette and vertical net stress evolution was monitored by a load cell. Time evolution of vertical net stress and degree of saturation changes on wetting are indicated in Fig. 2. Different patterns of behaviour are observed during this suction reduction path. The swelling pressure increases in the early transient stage to compensate for the swelling strain caused by the suction reduction, but eventually the sample yields. From the yield point on, the collapse tendency is compensated for by the expansion of the swelling microstructure, and the vertical stress reduces to maintain the constant volume condition. In this way, swelling stress reaches a maximum controlled by the LC yield surface, as explained by Alonso et al. (1990), and then decreases on subsequent wetting following approximately the yield locus at constant volume. The swelling pressure test results can be used to determine the saturated vertical preconsolidation stress $\sigma^*_{vo}=0.65$ MPa (point B in Fig. 2), as well as the initial yield point on the LC curve at $\sigma_{vo}=1.05$ MPa (point A in Fig. 2). This yield point is reached at an approximate degree of saturation of 70% (refer to Fig. 2). This degree of saturation is associated with a suction of $s=10$ MPa, which was measured with transistor psychrometers (Woodburn et al., 1993) on another sample undergoing the same fabrication and wetting process.

Based on this information, the LC yield locus, which represents the increase of preconsolidation stress with suction $\sigma_{vo}(s)$, is qualitatively depicted in Fig. 3 in conjunction with the stress paths previously described.

2.2. Controlled-suction technique and experimental setup

The vapour equilibrium technique was implemented by controlling the relative humidity of a closed system. In this way, soil water potential was applied

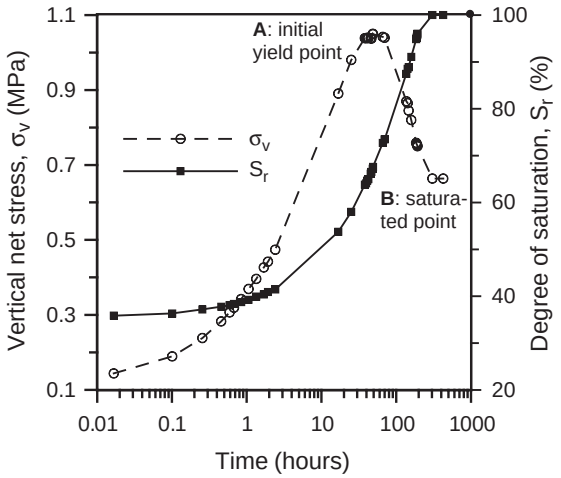

Fig. 2. Swelling pressure test.

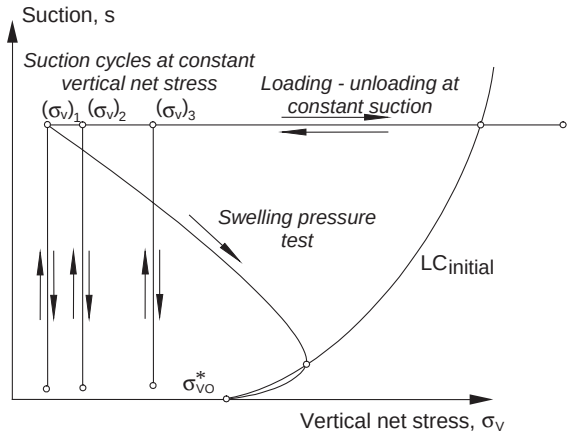

Fig. 3. Stress paths followed. Estimated LC yield locus for the as-compacted state.

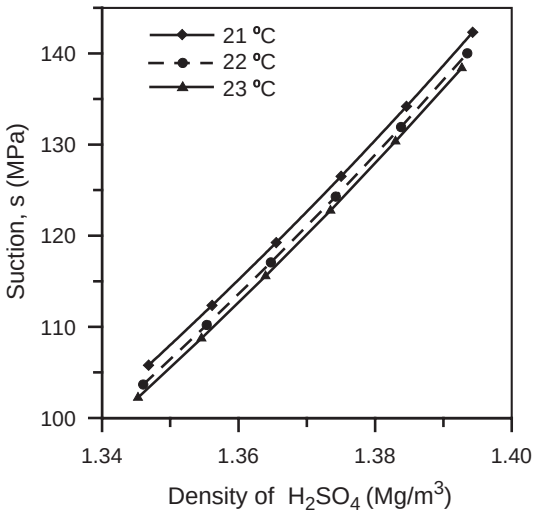

Fig. 4. Values of suction applied as a function of H_2SO_4 density and temperature.

by means of the migration of water molecules through the vapour phase from a reference system of known potential and mass to the soil pores, until hydro-mechanical equilibrium was achieved. The relative humidity of the reference system was controlled by varying the chemical potential of different types of aqueous solutions.

Non-volatile solutes ($CuSO_4$) and volatile solutes (acid solutions of H_2S0_4) were used in the experimental programme. $CuSO_4$ solutions were used under saturated conditions of dissolution, which allowed suctions ranging between 4 and 6 MPa to be attained. This procedure was used for the wetting paths. On the other hand, acid solutions were employed under partially saturated conditions of dissolution. In this case, a specified solute quantity was selected to achieve a target relative humidity of 40% (suction of $s=130$ MPa), which was used in the drying paths. However, the acid concentration was not fixed due to the fact that the soil exchanged vapour on drying with the reference system. A densimeter with a readability of 0.0005 Mg/m^3 was used to measure the equilibrated density of the solution after each drying path and at the controlled temperature of the laboratory. Fig. 4 shows the suction achieved as a function of the acid solution density and temperature. This plot is based on aqueous solution properties and the psychrometric law, which translates relative humidity values to suctions at a given temperature (Fredlund and Rahardjo, 1993). In addition, every new density was used to approximately determine, at a constant temperature, the amount of water lost by the soil on drying. Further details of this technique are presented in Romero (2001).

Each equalisation step was maintained until the rate of straining had reduced to an axial strain rate of 0.1%/day. Each drying–wetting step required a typical duration of 12 days, which resulted in a total test duration of approximately 4 months.

Fig. 5 shows the oedometer cell and the different elements of the controlled-suction technique. A forced convection system, driven by an air pump, was used to transport the vapour from the reference solution (desiccator in Fig. 5) to the soil pores. Mass exchanges were monitored by weighing the desiccator with an electronic balance with a resolution of 10 mg. Two procedures were followed to transfer the vapour: the vapour was either circulated along the boundaries of the sample (top and bottom porous stones indicated in Fig. 5) or it crossed the specimen. This last procedure of vapour transport through the sample (valves A and B closed, D and C open), which was used at low degrees of saturation, is more efficient but it is limited to soil states that present continuity of air. On the other hand, at higher degrees of saturation, the alternative procedure was followed (valves A and C closed, B and D open; or alternatively valves A, B and C open and D closed).

2.3. Stress paths followed

The different stress paths followed in this test programme are shown in Fig. 3 where tests are indi-

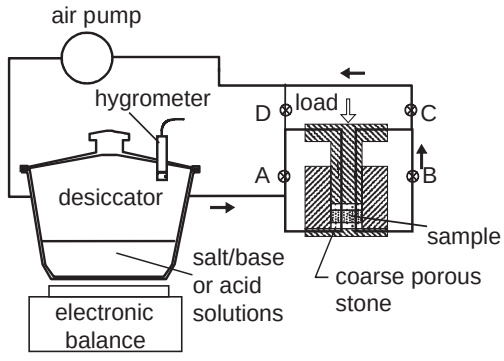

Fig. 5. Experimental setup of vapour equilibrium technique using a forced convection system.

cated in the (σ_v, s) plane. The drying–wetting paths were selected taking into account the position mapped for the LC curve from the auxiliary tests performed. Applied vertical stresses were in all cases lower than the yield stress for saturated conditions, σ^*_{vo}. The main reason for this, was to investigate the yield behaviour of the soil in the 'swelling region' far from the collapse mechanism, described by the LC curve. Three cyclic drying–wetting tests were performed at vertical net stresses of 98, 196 and 396 kPa respectively.

Once the sample was compacted in the oedometer cell, the selected vertical load was applied. Suction was maintained at a value of $s = 80$ MPa. Once equilibrium was reached the first wetting cycle was applied. Suction was reduced in a single step, to a value in the range 4–6 MPa. Subsequent drying–wetting reversals were then applied once equilibrium was reached. Suction was changed in a single step from a low value of 4–6 MPa to a high value of 120–135 MPa. The exact suction depended on the room temperature and the concentration of the solution used. Five to six cycles were applied for each vertical stress.

The constitutive model that was used as a reference framework is presented prior to discussing the test results in more detail.

3. Expansive model. Theoretical framework for isotropic states

3.1. Elastic behaviour

Two structural levels are distinguished in the fabric of an expansive soil: micro and macro (Gens and Alonso, 1992). The microstructural level describes the aggregates of active clay minerals and is associated with the lower range of soil pores. Its volume is given by the microstructural void ratio, e_m. Clay fabric at this level is assumed to react in a pure volumetric and elastic manner against changes in isotropic stress and suction (Alonso et al., 1999):

$$d\varepsilon^e_{vm} = \frac{d\hat{p}}{K_m} \tag{1}$$

where $d\varepsilon^e_{vm} = -de_m/(1+e_m)$ is the elastic microstructural volumetric strain, K_m is a compressibility coefficient and $\hat{p}$ is a generalised microstructural effective stress, defined as:

$$\hat{p} = p + S^{\alpha}_{rmic} s \tag{2}$$

where p is the mean net stress (excess of average total mean stress over air pressure), s is the suction, S_{rmic} is the degree of saturation of the microstructural level (which depends on s) and α is a constitutive coefficient. When $\alpha = 0$, saturated effective stress is recovered. When $\alpha = 1$, $\hat{p}$ corresponds to Bishop's mean stress.

The coefficient K_m is not a constant. It depends on the confining stress. A suitable expression for K_m is derived from the classical logarithmic law of void ratio reduction for increasing stress:

$$K_m = \frac{(1+e_m)\hat{p}}{\kappa_m} \tag{3}$$

where κ_m is the (constant) compressibility index of the microstructure.

Macrostructural strains describe the rearrangement of the soil structure. They imply changes in size of the largest pore sizes, characterised by a global volume measure (macrostructural void ratio e_M; the void ratio is then given by $e = e_m + e_M$). Elastic and plastic macrostructural strains develop as stress and suction change. Elastic macro strains are given by the classical expression of Alonso et al. (1990):

$$d\varepsilon^e_{VM} = \frac{dp}{K_t} + \frac{ds}{K_s} \tag{4}$$

where

$$K_t = \frac{(1+e_M)p}{\kappa} \qquad K_s = \frac{(1+e_M)(s+p_{atm})}{\kappa_s} \tag{5}$$

and κ and κ_s are (macro) compressibility indexes against mean net stress and suction changes.

The total elastic strain can be calculated using

$$d\varepsilon^e_v = d\varepsilon^e_{vm} + d\varepsilon^e_{vM} \tag{6}$$

3.2. Plastic behaviour

The variation of preconsolidation mean net stress with suction is given by an LC yield surface in the (p, s) plane:

$$p_0 = p_c \left(\frac{p^*_o}{p_c}\right)^{\frac{\lambda(0)-\kappa}{\lambda(s)-\kappa}} \tag{7}$$

with

$$\lambda(s) = \lambda(0)\left[r + (1-r)e^{-\beta s}\right] \quad (8)$$

where p_o^* is the saturated preconsolidation mean net stress, p_c is a reference stress, $\lambda(0)$ is the slope of the virgin compression line and (r, β) are model parameters.

Eq. (7) describes the yield conditions of the macrostructure. Experimental evidence, reported in the Introduction of this paper, indicates that wetting and drying paths are also capable of inducing plastic strains. These plastic strains have their origin in the underlying microstructural deformations but, as reported previously, they seem to be controlled also by the applied confining stress and by the density (alternatively, the intensity of compaction) of the material. The model describes the plastic straining by means of two additional yield curves (SI and SD, associated with suction increase and suction decrease, respectively), which are represented in Fig. 6. These yield curves are defined by the expressions $\hat{p} - s_I = 0$ for the SI yield curve and $\hat{p} - s_D = 0$ for the SD yield curve; s_I, s_D being the hardening parameters.

When SI and SD yield curves are activated, plastic strains are induced, which in view of the above considerations have been given the following expressions:

$$d\varepsilon_{vM}^p = f_I\, d\varepsilon_{vm}^e \quad (9)$$

$$d\varepsilon_{vM}^p = f_D\, d\varepsilon_{vm}^e \quad (10)$$

f_I and f_D are micro–macro coupling functions which are made dependent on (p/p_0), p_0 being the current preconsolidation stress at the current value of suction, as given by the LC yield curve. The nature of these coupling functions will be discussed later when the experimental results are analysed.

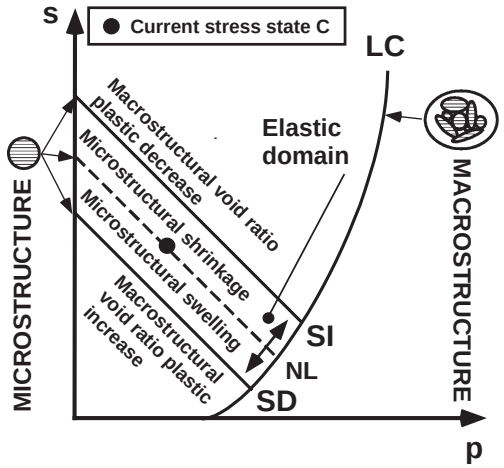

Fig. 6. Yield loci of expansive model.

It was also assumed that SI and SD hardening is governed by $d\alpha_1 = d\varepsilon_{vSI}^p + d\varepsilon_{vSD}^p$, although a dependence on plastic strains induced by LC plastic loading may be suspected. LC hardening is assumed to depend on $d\alpha_2 = d\varepsilon_{vSI}^p + d\varepsilon_{vSD}^p + d\varepsilon_{vLC}^p$, where $d\varepsilon_{vLC}^p$ is the volumetric plastic strain due to the activation of LC. Hardening laws are defined as follows (Alonso et al., 1999):

$$ds_I = \frac{K_m d\alpha_1}{f} = ds_D \quad (11)$$

$$\frac{dp_0^*}{p_0^*} = \frac{(1+e_M)d\alpha_2}{\lambda(0)-\kappa} \quad (12)$$

In Eq. (11) the function f is either f_I or f_D depending on whether yielding is occurring on the SI or SD curve.

4. Test results and interpretation

4.1. Complementary tests

In the remainder of the paper, the mean net stress p in the model will be replaced by the applied vertical net stress σ_v. Since horizontal stresses were not measured, application of a generalised model would not lead to significant advantages over the simpler approach adopted.

The swelling pressure test provides direct information on the value of the saturated preconsolidation stress σ_{vo}^* and on the shape of the LC yield locus of the macrostructure. Gens and Alonso (1992) showed that the maximum swelling pressure is slightly above the current yield stress for the prevailing suction. In addition, the swelling pressure path for lower suction values follows approximately the LC yield curve. The recorded data given in Fig. 2 has been used to plot the swelling pressure path in a (σ_v, s) stress plane. Measured degrees of saturation (or alternatively, water content w) were related to suction through the following empirical relationship found by Villar (1995) for the water retention curve of the FEBEX bentonite:

$$w = 36 - 5.5\ln(s); w \text{ in \% and } s \text{ in MPa} \quad (13)$$

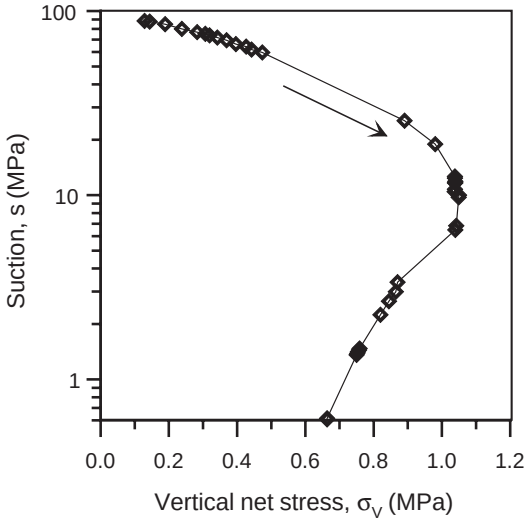

Fig. 7. Swelling pressure path.

The swelling pressure path was derived using the above equation. It has been plotted in Fig. 7. The yield stress (σ_{vo}=5 MPa in Fig. 1) derived from the compression test at a constant suction s= 80 MPa provides another point of the LC yield curve. The post-yield compression index, $\lambda(s)$, for s=80 MPa ($\lambda(s)$=0.22) and the elastic compressibility index κ (κ=0.008), were additionally determined.

The set of data derived from the compression at constant suction and the swelling pressure test provide enough data to derive all the parameters, which define the LC yield locus (Eqs. (7) and (8)) (Table 1).

The LC yield locus for as-compacted conditions is plotted in Fig. 8. It shows the marked effect of suction on the apparent preconsolidation stress of the compacted 80/20 bentonite–sand mixture.

Table 1
Parameters of the LC yield curve (macrostructure)

Parameter	Description	Value
σ^*_{vo}	Saturated yield stress	650 kPa
p_c	Reference stress	0.008 kPa
$\lambda(0)$	Saturated virgin compression index	0.25
κ	Elastic (unloading–reloading) compression index	0.008
β	Parameter which defines the curvature of the LC yield curve	0.05 MPa^{-1}
r	Parameter which defines the limiting value of the compression index for high suctions	0.85

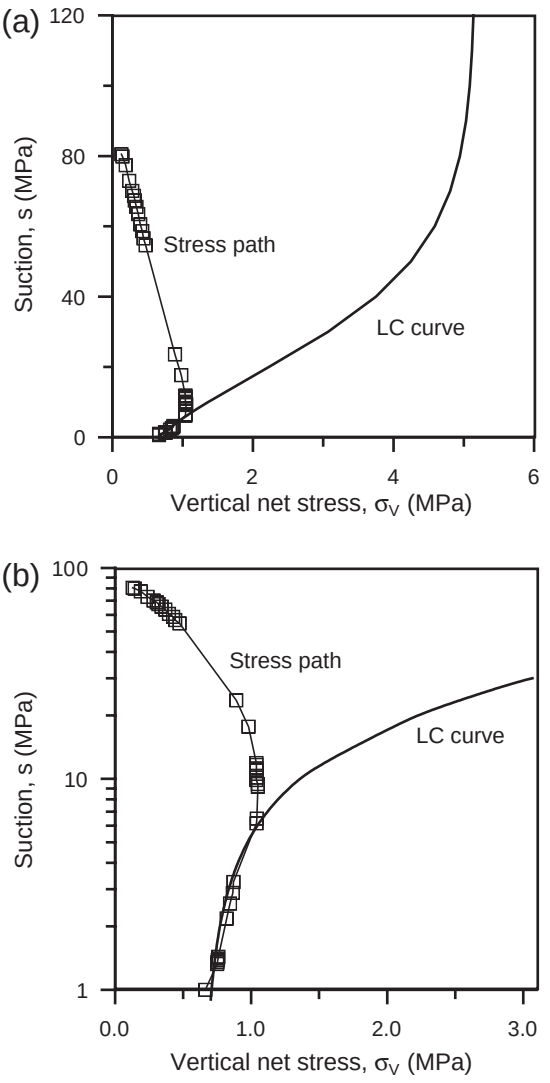

Fig. 8. Derived LC yield curve and stress path followed by the swelling pressure test: (a) natural scale, (b) log scale (zoom in the vicinity of the saturated zone).

4.2. Cyclic controlled-suction tests

Volumetric deformations for the three series of tests performed have been plotted in Figs. 9–11 for the three applied vertical stresses (compressive strains are plotted as positive). The first wetting path results in all cases in sample expansion. However, as the subsequent drying–wetting cycles are applied there is in general a net accumulation of sample compression. The exception is the first cycle of the test series for

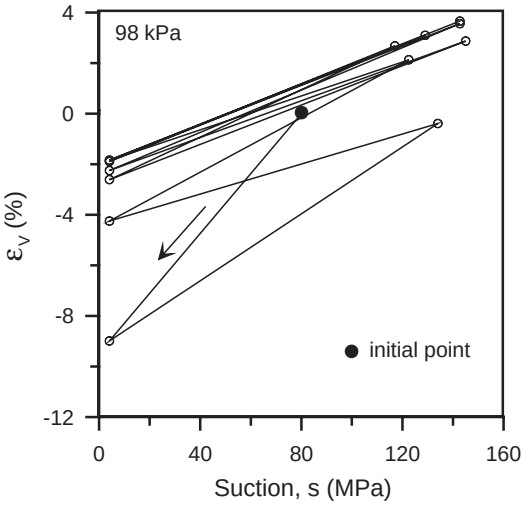

Fig. 9. Volumetric deformations in cyclic controlled-suction paths, σ_v=98 kPa.

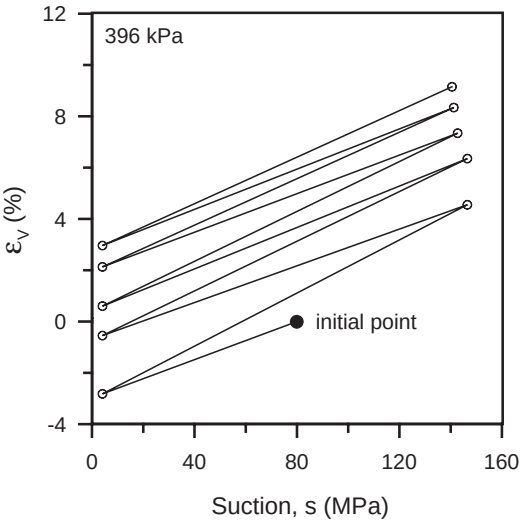

Fig. 11. Volumetric deformations in cyclic controlled-suction paths, σ_v=396 kPa.

the lowest applied vertical stress–or highest OCR–(σ_v=98 kPa; Fig. 9). As the number of cycles increases the differences between two successive wetting–drying paths become smaller. Clearly, the soil tends towards an 'elastic' (reversible) state. This trend is better appreciated if the volumetric strains either in expansion or compression are plotted as the number of cycles increases. This is done in Fig. 12 for the test series σ_v=196 kPa. The difference, a net compression, tends to zero as the number of cycles increases. This limiting value, which is not strictly reached for the number of cycles applied in these experiments, marks a stable elastic state, which may be approximately taken as the state for the last suction change applied.

The data presented in Figs. 9–11 and the interpretation given above provide data to investigate the capability of the theoretical framework described before to model the soil behaviour against suction changes. Note that, once the elastic components are substracted from

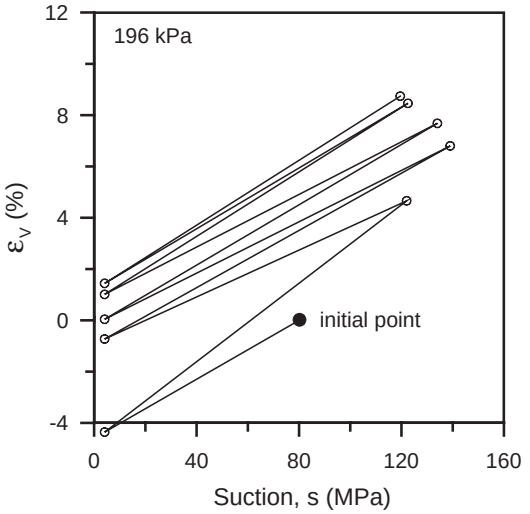

Fig. 10. Volumetric deformations in cyclic controlled-suction paths, σ_v=196 kPa.

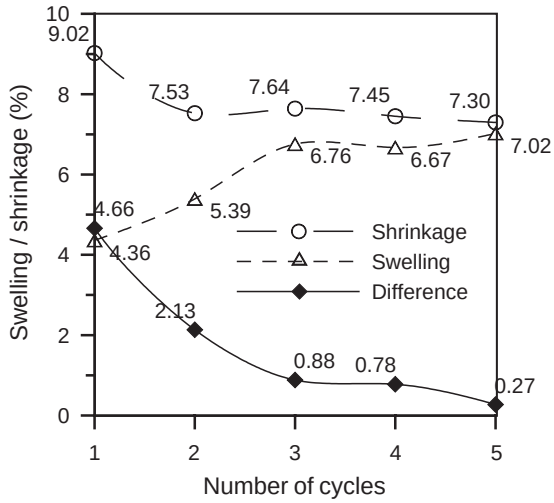

Fig. 12. Evolution of swelling and shrinkage with the number of controlled-suction cycles (σ_v=196 kPa).

the total strains given in Figs. 9–11, plastic components may be obtained and their evolution with the applied suction cycles could be investigated. Therefore, the evolution of the coupling functions as defined in Eqs. (9) and (10) could be investigated. Before this is done, however, some simplifications have been introduced into the theoretical framework in order to facilitate parameter determination.

4.3. Model simplification and parameter determination. Micro–macro interaction

Since the elastoplastic model is formulated in differential terms, the stress paths applied in experiments should ideally be performed in small incremental steps. However, in highly plastic expansive materials such as the bentonite–sand mixtures, the time to equalize a given suction or stress change is very large for the typical size of the oedometer (or triaxial) specimen. If the large suction changes applied had to be divided into several steps the time length of these tests would have been exceedingly large. On the other hand, the large suction changes make it difficult to apply in a direct manner, the constitutive relations presented before.

The number of couplings between different aspects of behaviour also makes it difficult to adopt a simple systematic procedure to derive model parameters. Since this is always a desirable feature it was decided to introduce some simplifications even if some model capabilities are reduced.

Accordingly, the following simplifying assumptions were introduced:

- Microstructural deformations will be governed by changes in saturated effective stress ($p+s$). This assumption implies a fully saturated microstructure $S_{rmic}=1$ and eliminates the need to introduce the water retention curve and the parameter α ($S_{rmic}^{\alpha}=1$ in Eq. (2)).
- Suction-induced elastic deformations are considered only as microstructural deformations, i.e. any suction-induced macrostructural elastic deformations are ignored ($\kappa_s=0$ in Eq. (5)).
- It will be assumed that the SI and SD yield surfaces are always activated as suction changes during the application of drying–wetting cycles. In other words, the elastic region bounded by SI and SD is assumed to be negligible ($s_I=s_D$ in Fig. 6). This assumption facilitates the computation of plastic strains.

The first two assumptions, together with Eqs. (1) (2) and (3) result in the following expression for the elastic volumetric strain induced by a change in suction from an initial value s_i to a final value s_f:

$$\Delta\,\varepsilon_{vm}^{e}=\frac{\kappa_m}{1+e_0}\ln\left(\frac{p+s_f}{p+s_i}\right) \tag{14}$$

Then, the microstructural elastic parameter κ_m could be determined for the equilibrium (final) stage of the application of several suction cycles. The above described procedure was used to derive the microstructural elastic index for each of the three vertical stresses applied, which is plotted in Fig. 13. Probably, the low value recorded for the low applied stress ($\sigma_v=98$ kPa) is explained by friction forces at the contact between sample and confining ring. Therefore, a decrease of the elastic compressibility coefficient with applied stress, which is also shown in Fig. 13, is considered more realistic. In fact, the volumetric deformations recorded during the first wetting path (Fig. 14) follow an expected decay of deformation with applied stress.

Eq. (14) also provides a procedure to obtain the elastic strains for intermediate cycles characterised by different s_i and s_f values. Plastic strains induced by the imposed changes in suction can now be computed as well as the interaction functions f_D and f_I defined in

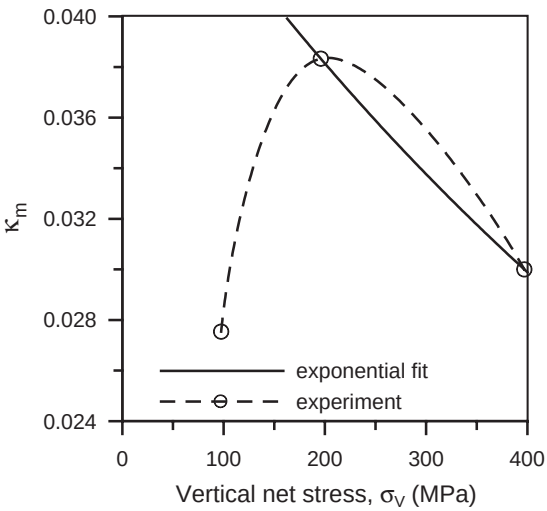

Fig. 13. Elastic compression index for the last suction path applied.

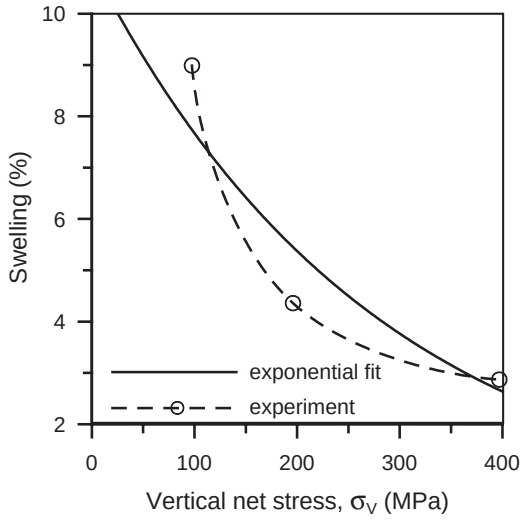

Fig. 14. Variation of swelling strains with applied confining stress for the first wetting path applied.

Eqs. (9) and (10). The evolution of plastic volumetric strains with the number of applied suction cycles for σ_v=396 kPa is plotted in Fig. 15. Functions f_D and f_I should be related to the ratio σ_v/σ_{vo}, where σ_v is the current vertical stress and σ_{vo} is the current preconsolidation stress at the current value of suction. The large suction steps applied make it difficult to calculate the appropriate σ_{vo} value. In the simplified version applied here it was decided to substitute the varying σ_{vo} value by the saturated preconsolidation stress σ^*_{vo}. The initial value of σ^*_{vo} was taken as the swelling pressure under saturated conditions reported in Fig. 7 for the as-compacted conditions. Subsequent changes in σ^*_{vo} could be found through the hardening Eq. (12) and the measured plastic strains, which imply:

$$\frac{\Delta\sigma^*_{vo}}{\sigma^*_{vo}} = (1+e)\frac{\Delta\varepsilon^p_v}{(\lambda(0)-\kappa)} \qquad (15)$$

Summarising the calculation of the interaction functions, on the basis of applied suction cycles, follows the following procedure:

– Elastic parameters are first computed. κ_m is derived from the final (elastic) suction cycle applied or, better for the extrapolated elastic behaviour of the soil when irreversible swelling or shrinkage strains are negligible. The microstructure is assumed saturated and Eq. (14) applies.
– Elastic (microstructural) strains are computed for every suction cycle (through Eq. (14)), once κ_m is obtained.
– Plastic deformations are derived for each suction cycle by subtracting elastic strains from total strains.
– Values of σ_v/σ^*_{vo} are derived for each suction cycle. σ_v is the applied vertical stress. σ^*_{vo} is taken, initially (first cycle), as the swelling pressure. Subsequent changes in σ^*_{vo} are determined from Eq. (15).
– The ratio: (plastic strain/(microstructural) elastic strain) is plotted against σ_v/σ^*_{vo} for each suction step. The experimental interaction functions (for drying and wetting changes) are thus derived.

Following this procedure, the calculated f_D and f_I values have been plotted in Fig. 16 against the ratio σ_v/σ^*_{vo}. The plots for σ_v=396 and 196 kPa show that f_D and f_I tend to converge to a common value f_D=f_I=0, which will mark the long term stable point for an infinite number of suction cycles. In these two cases the path followed by the point that describes the state of the soil moves towards the left (increasing σ^*_{vo} values, i.e.: a denser structure as a result of the accumulated shrinkage). This trend is not so clear for the specimen under σ_v=98 kPa, because the long term equilibrium value of σ_v/σ^*_{vo} is close to the initial value of σ_v/σ^*_{vo} for this (lower) applied confining stress (i.e. for a high OCR).

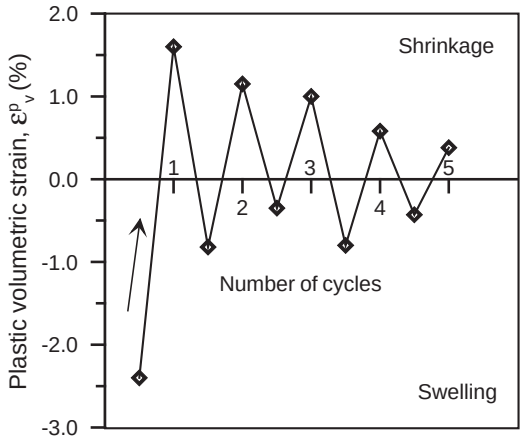

Fig. 15. Computed plastic volumetric strains and its evolution with the number of cycles (σ_v=396 kPa).

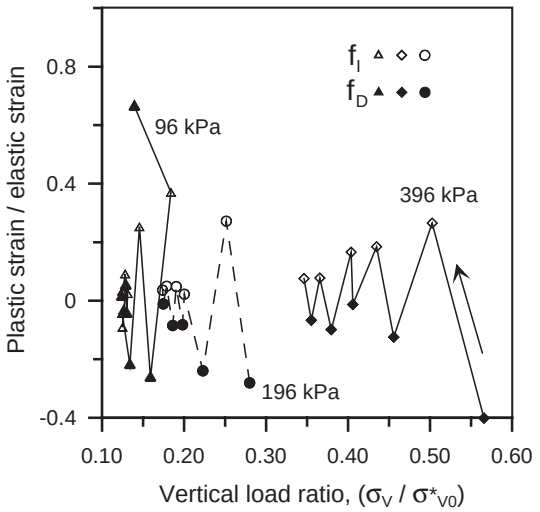

Fig. 16. Experimental values of the interaction functions f_D and f_I.

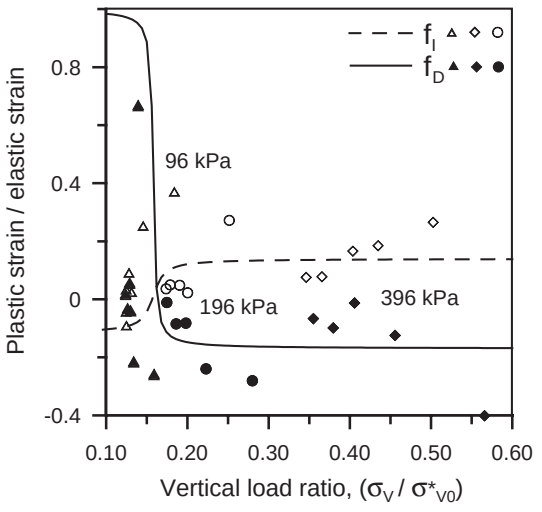

Fig. 17. Comparison between theoretical interaction functions and experimental values.

The set of experimental points given in Fig. 16 has been approximated by sigmoidal functions:

$$f_I = \frac{f_{I1} - f_{I2}}{\pi} \tan^{-1}\left[K_I\left(\frac{\sigma_v}{\sigma^*_{vo}} - X_I\right)\right] + \frac{f_{I1} + f_{I2}}{2} \quad (16)$$

$$f_D = \frac{f_{D1} - f_{D2}}{\pi} \tan^{-1}\left[K_D\left(\frac{\sigma_v}{\sigma^*_{vo}} - X_D\right)\right] + \frac{f_{D1} + f_{D2}}{2} \quad (17)$$

A minimum accumulated error square fit leads to the functions plotted in Fig. 17. Parameters of Eqs. (16) and (17) are given in Table 2.

5. Comparison of model predictions and test results

The three tests performed have been simulated with a common set of model parameters, given before. In performing the model simulations f_I and f_D have been taken as functions of σ_v/σ^*_{vo}, as was previously assumed in deriving the functions from the experimental data. Complete information is given in Fig. 18 for the test under $\sigma_v = 196$ kPa in terms of:

- Comparison of actual deformations with model calculations.
- Evolution of the micro/macro interaction, as defined by the interaction functions f_D and f_I.
- Evolution of the LC yield curves as the soil densifies.

The correspondence between measured and predicted deformations is reasonably good (Fig. 18a). Fig. 18b indicates the progressive approximation of the sample state towards the crossing point of the f_D, f_I functions. This approximation towards the left implies an increasing value of preconsolidation stress, i.e. a soil densification. Soil densifies because the f_I values for a given σ_v/σ^*_{vo} value, are larger than f_D values (irreversible shrinkage overcomes irreversible expansion).

This is also reflected in the third plot (Fig. 18c), which shows the evolution of the LC value towards increasing values of σ_v, enlarging the elastic region (a progressively denser soil).

Table 2
Parameters of interaction functions (Eqs. (16) and (17))

Function f_I		Function f_D	
Parameter	Value	Parameter	Value
f_{I1}	−0.12	f_{D1}	1
f_{I2}	0.14	f_{D2}	−0.17
K_I	100	K_D	400
X_I	0.158	X_D	0.158

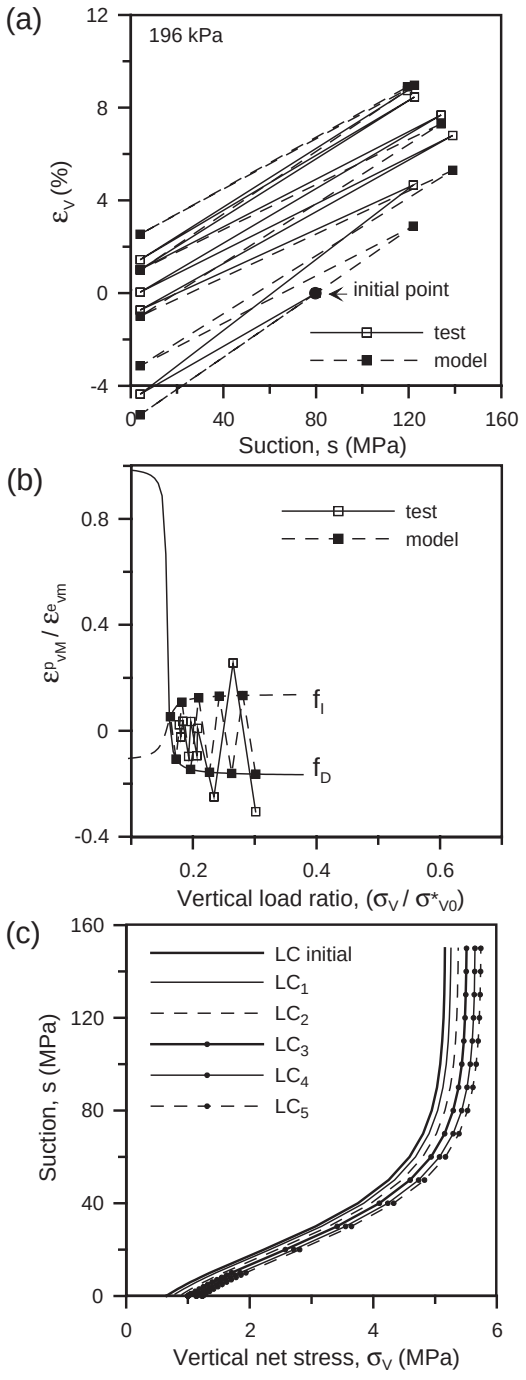

Fig. 18. Controlled-suction cyclic test for σ_v=196 kPa. (a) Comparison of test results and model predictions. (b) Evolution of micro–macro interaction in terms of the coupling functions f_D and f_I. (c) Evolution of the LC curve.

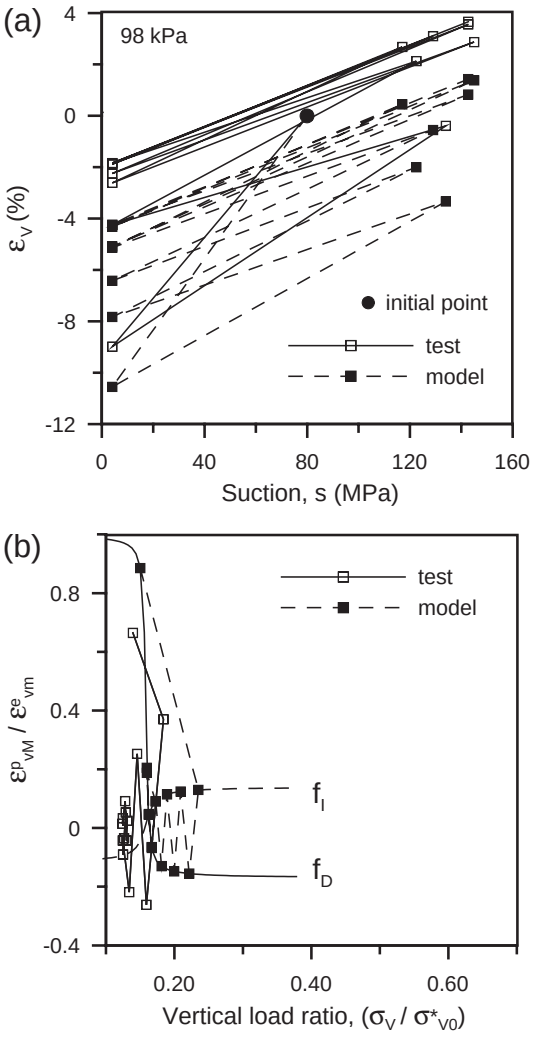

Fig. 19. Controlled-suction cyclic tests for σ_v=98 kPa. (a) Comparison of test results and model predictions. (b) Evolution of micro–macro interaction in terms of the coupling functions f_D and f_I.

Similar plots are given in Figs. 19 and 20 for σ_v=98 kPa and σ_v=396 kPa, respectively. The comparison between model and experimental results is particularly good for σ_v=396 kPa (Fig. 20a). However, the comparison is not so good for σ_v=98 kPa (Fig. 19). It is interpreted that the state of the sample for σ_v=98 kPa is on the left of the critical equilibrium point (f_D=f_I). A first expansion takes the sample to the 'shrinkage' region and it evolves by accumulating irreversible shrinkage as the number of cycles increases.

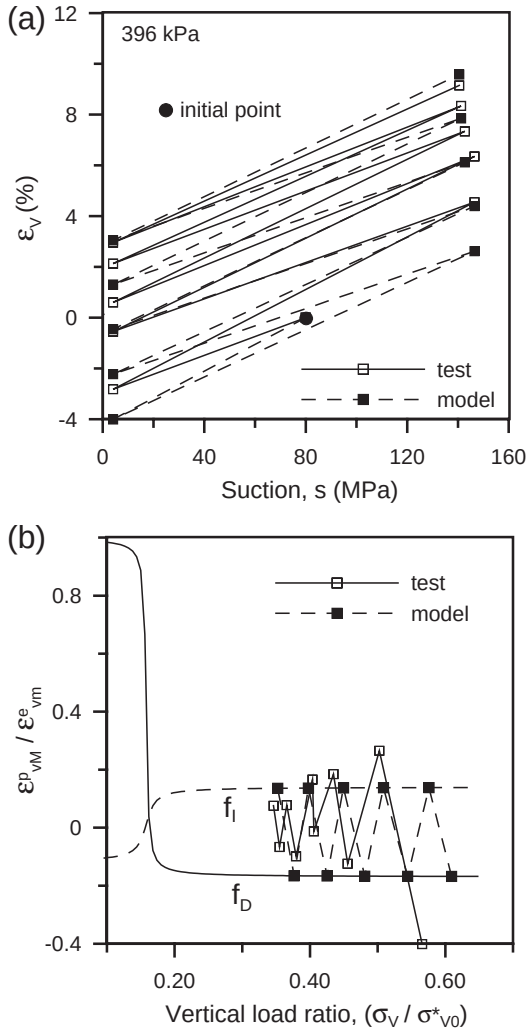

Fig. 20. Controlled-suction cyclic test for σ_v=396 kPa. (a) Comparison of test results and model predictions. (b) Evolution of micro–macro interaction in terms of the coupling functions f_D and f_I.

Discrepancies may be associated with the proximity of the soil state to the critical $f_D = f_I$ point but, also, to more complex stress states within the sample such as the effects of side friction.

6. Summary and conclusions

The effect of applying wetting–drying suction cycles on an expansive bentonite–sand (80/20) compacted mixture has been investigated. The mixture was statically compacted to a dry density of 1.5 Mg/m^3 and a degree of saturation close to 0.35. Suction cycles were applied by means of vapour equilibrium technique in an oedometer cell. The range of suctions applied (130–4 MPa) was large. The vertical confining stress was kept constant during each series of suction reversals. The initial overconsolidation ratio (OCR), taking as a reference the saturated preconsolidation stress (estimated from the swelling pressure), varied between 1.6 and 7. It was observed that samples experienced a progressive shrinkage as the suction cycles accumulate. Eventually a reversible elastic response was approached. This progressive shrinkage process led to an increase of the OCR.

Test results have been interpreted within the framework of an elastoplastic constitutive model (BExM) described in Alonso et al. (1999), which uses a double structure approach and is briefly outlined in the paper. The paper describes in detail the process of parameter determination. In this regard, two auxiliary tests were also performed: a swelling pressure test and a compression test under constant suction. Both tests provide enough information to quantify the macrostructural parameters of BExM. A procedure to derive the microstructural parameters and to interpret the mechanical interaction between both structural levels has been proposed. Some simplifications of the original model proposed by Alonso et al. (1999) have been introduced to facilitate this task. A single set of material constants was derived on the basis of all the tests performed. Finally model 'predictions' were compared with actual volumetric deformations measured during the application of suction cycles. There is a reasonably good agreement, although some difficulties were met to reproduce the test performed at the lower vertical stress.

Two additional aspects should be mentioned. The low permeability of the tested material leads to very long equilibration times even with some special testing techniques (circulation of controlled vapour through the sample). The tests reported here lasted for several months. It is thus essential for these materials to find procedures to derive constitutive parameters using a minimum number of different stress paths applied. The discussion made in the paper should be useful for planning future studies successfully. Finally, the application of suction cycles repro-

duces a situation that is often encountered in practice. But it should be also viewed as a procedure to derive key parameters of the theory developed and, more specifically, of the microstructural behaviour and its effect on observed irreversible deformations.

Acknowledgements

The authors acknowledge the financial support provided to the third author by AECI (Agencia Española de Cooperación Iberoamericana) and Universidad de La República (Uruguay). The support of DGICYT through research grant PB98-0918 is also acknowledged. The comments made by the reviewers of the paper were greatly appreciated.

References

Al-Homoud, A.S., Basma, A.A., Husein Malkawi, A.I., Al-Bashabsheh, M.A., 1995. Cyclic swelling behaviour of clays. J. Geotech. Eng., vol. 121 (7). ASCE, pp. 562–565.

Alonso, E.E., Gens, A., Josa, A., 1990. A constitutive model for partially saturated soils. Geotechnique 40 (3), 405–430.

Alonso, E.E., Vaunat, J., Gens, A., 1999. Modelling the mechanical behaviour of expansive clays. Eng. Geol. 54, 173–183.

Basma, A.A., Al-Homoud, A.S., Husein Malkawi, A.I., Al-Bashabsheh, M.A., 1996. Swelling-shrinkage behavior of natural expansive clays. Appl. Clay Sci. 11 (2–4), 211–227.

Day, R.W., 1994. Swell-shrink behavior of compacted clay. J. Geotech. Eng., vol. 120 (3). ASCE, pp. 618–623.

Dif, A.E., Bluemel, W.F., 1991. Expansive soils under cyclic drying and wetting. Technical note. Geotech. Test. J. 14 (1), 96–102 (GTJODJ).

ENRESA (2000). FEBEX Project. Full-scale engineered barriers experiment for a deep geological repository for high level radioactive waste in crystalline host rock. Final Report. Publicación Técnica ENRESA 1/2000, Madrid.

Fredlund, D.G., Rahardjo, H., 1993. Soil Mechanics for Unsaturated Soils. John Wiley & Sons, Inc., New York.

Gens, A., Alonso, E.E., 1992. A framework for the behaviour of unsaturated expansive clays. Can. Geotech. J. 29, 1013–1032.

Obermeier, S.F., 1973. Evaluation of laboratory techniques for measurement of swell potential of clays. Proc. Workshop on Expansive Clays and Shales in Highway Design and Construction, vol. 1, pp. 214–254.

Popescu, M., 1980. Behaviour of expansive soils with a crumb structure. Proc. 4th Int. Conf. on Expansive Soils. Denver, Colorado, vol. 1, pp. 158–171.

Pousada, E., (1984). *Deformabilidad de arcillas expansivas bajo succión controlada*. Doctoral Thesis. Universidad Politécnica de Madrid, Spain.

Romero, E., 2001. Controlled-suction techniques. In: Gehling, W.Y.Y., Schnaid, F. (Eds.), Proc. 4° Simpœsio Brasileiro de Solos Nâo Saturados, Porto Alegre. Associação Brasileira de Mecânica dos Solos e Engenharia Geotécnica ABMS, Porto Alegre, Brasil, pp. 535–542.

Villar, M.V., 1995. First results of suction controlled oedometer test in highly expansive montmorillonite. In: Alonso, E.E., Delage, P. (Eds.), Proc. 1st Int. Conf. on Unsaturated Soils, Paris, vol. 1. Balkema/Presses des Ponts et Chaussées, pp. 207–213.

Woodburn, J.A., Holden, J., Peter, P., 1993. The transistor psychrometer: a new instrument for measuring soil suction. In: Houston, S.L., Wray, W.K. (Eds.), Unsaturated Soils Geotechnical Special Publications No. 39, Dallas. ASCE, pp. 91–102.